ACS central science

http://pubs.acs.org/journal/acscii

Research Article

Near-Infrared Light Responsive Nanoreactor for Simultaneous Tumor Photothermal Therapy and Carbon Monoxide-Mediated Anti-Inflammation

Shi-Bo Wang,[#] Cheng Zhang,[#] Jing-Jie Ye, Mei-Zhen Zou, Chuan-Jun Liu, and Xian-Zheng Zhang*

Cite This: *ACS Cent. Sci.* 2020, 6, 555−565

Read Online

ACCESS | Metrics & More | Article Recommendations | Supporting Information

ABSTRACT: Photothermal therapy (PTT) is an effective treatment modality with high selectivity for tumor suppression. However, the inflammatory responses caused by PTT may lead to adverse reactions including tumor recurrence and therapeutic resistance, which are regarded as major problems for PTT. Here, a near-infrared (NIR) light-responsive nanoreactor (P@DW/BC) is fabricated to simultaneously realize tumor PTT and carbon monoxide (CO)-mediated anti-inflammatory therapy. Defective tungsten oxide (WO_3) nanosheets (DW NSs) are decorated with bicarbonate (BC) via ferric ion-mediated coordination and then modified with polyethylene glycol (PEG) on the surface to fabricate PEG@DW/BC or P@DW/BC nanosheets. Upon 808 nm NIR laser irradiation, the DW content in P@DW/BC can serve as not only a photothermal agent to realize photothermal conversion but also a photocatalyst to convert carbon dioxide (CO_2) to CO. In particular, the generated heat can also trigger the decomposition of BC to produce CO_2 near the NSs, thus enhancing the photocatalytic CO generation. Benefiting from the efficient hyperthermia and CO generation under single NIR laser irradiation, P@DW/BC can realize effective thermal ablation of tumor and simultaneous inhibition of PTT-induced inflammation.

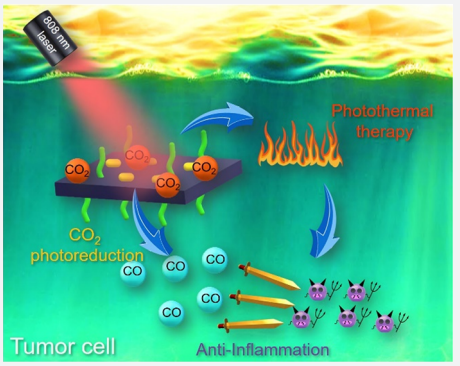

INTRODUCTION

Photothermal therapy (PTT) that utilizes near-infrared (NIR) light-absorbing agents to convert photoenergy into heat for cells thermal ablation is regarded as a minimally invasive and highly efficient treatment approach for tumor management.[1−3] Owing to the good controllability of NIR light (e.g., power density, duration, and range) and the negligible toxicity of photothermal agents (PTAs) in the dark, PTT can eliminate tumor cells specifically without harming normal tissues, which is a promising alternative to traditional tumor therapy.[4,5] However, because of the hyperthermia induced by PTAs, the most possible cellular death mode after PTT is necrosis, which is characterized by rupture of the plasma membrane, release of cellular contents, and in turn an introduction of inflammation.[6,7] Although inflammation is a common defensive response of the body to external stimuli, it has been shown that the therapy-induced inflammation might cause severe adverse effects, including tumor regeneration, metastatic dissemination, and therapeutic resistance.[8−11] Therefore, effective alleviation of inflammatory responses caused by PTT is of great significance for tumor treatment.

Carbon monoxide (CO), a colorless and odorless gas, is increasingly appreciated as a crucial signaling molecule and has been proved to hold substantial therapeutic potentials in cytoprotection, hypertension management, bacterial inhibition, and chemosensitization.[12−15] Moreover, CO has also been confirmed as an effective agent for anti-inflammation.[16−18] In light of this, combining CO with PTT might be a feasible way to reduce the therapy-induced inflammation. However, because of the great affinity between CO and hemoglobin, the direct use of gaseous CO is risky and lacks tumor selectivity. Therefore, developing advanced strategies to realize *in situ* CO generation in tumor tissues is necessary for the combination between PTT and CO. Recently, photocatalytic CO_2 reduction has been confirmed as a promising way to realize *in vivo* CO generation.[19,20] By regulating external light irradiation, the CO generation can be accurately adjusted, which makes it an attractive method for *in situ* CO production. However, current studies mainly depended on a visible-light-responsive photocatalyst to convert internal CO_2 to CO *in vivo*.[19,20] The limited penetration ability of visible light in biological tissues severely prevents the CO production in deep tissues. Moreover, the concentration of internal CO_2 is always relatively low, and the strong dependence on internal CO_2 also seriously hinders the efficient CO_2 photoreduction *in vivo*. Thus, developing novel photocatalytic CO generation systems to overcome these problems is an urgent need.

Received: December 31, 2019
Published: March 23, 2020

https://dx.doi.org/10.1021/acscentsci.9b01342
ACS Cent. Sci. 2020, 6, 555−565

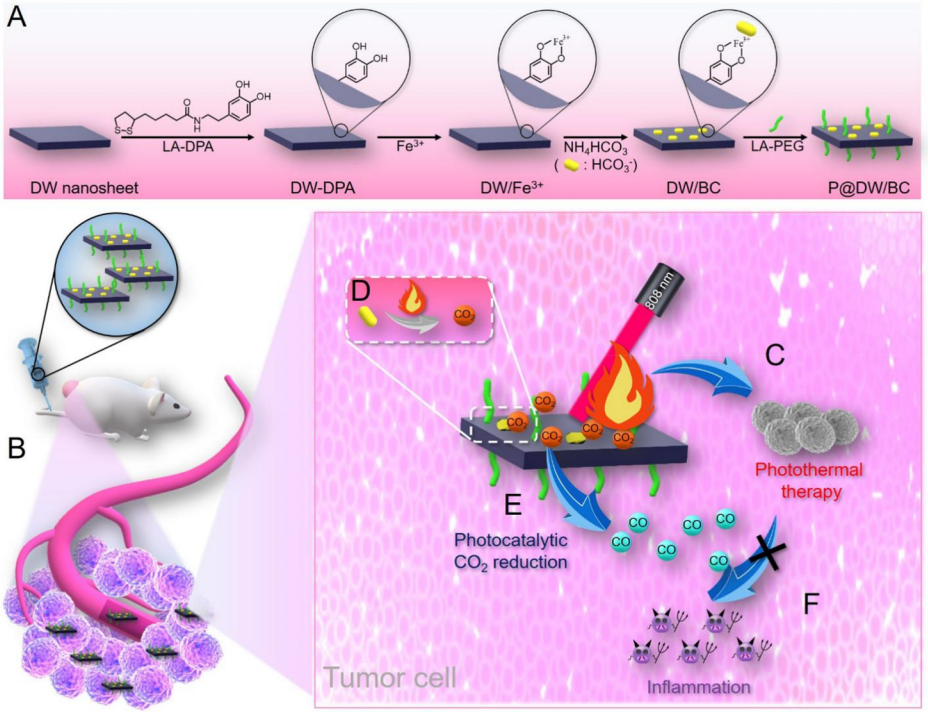

Figure 1. Schematic illustration of P@DW/BC NSs for simultaneous tumor PTT and anti-inflammation. (A) Preparation process for P@DW/BC NSs. (B) Selective accumulation of P@DW/BC NSs in tumor after intravenous injection via the EPR effect. (C) P@DW/BC NSs-mediated PTT for tumor inhibition. (D) Heat-triggered BC decomposition to produce CO_2. (E) P@DW/BC NSs-mediated photocatalytic CO_2 reduction to produce CO. (F) Elimination of PTT-caused inflammation by CO.

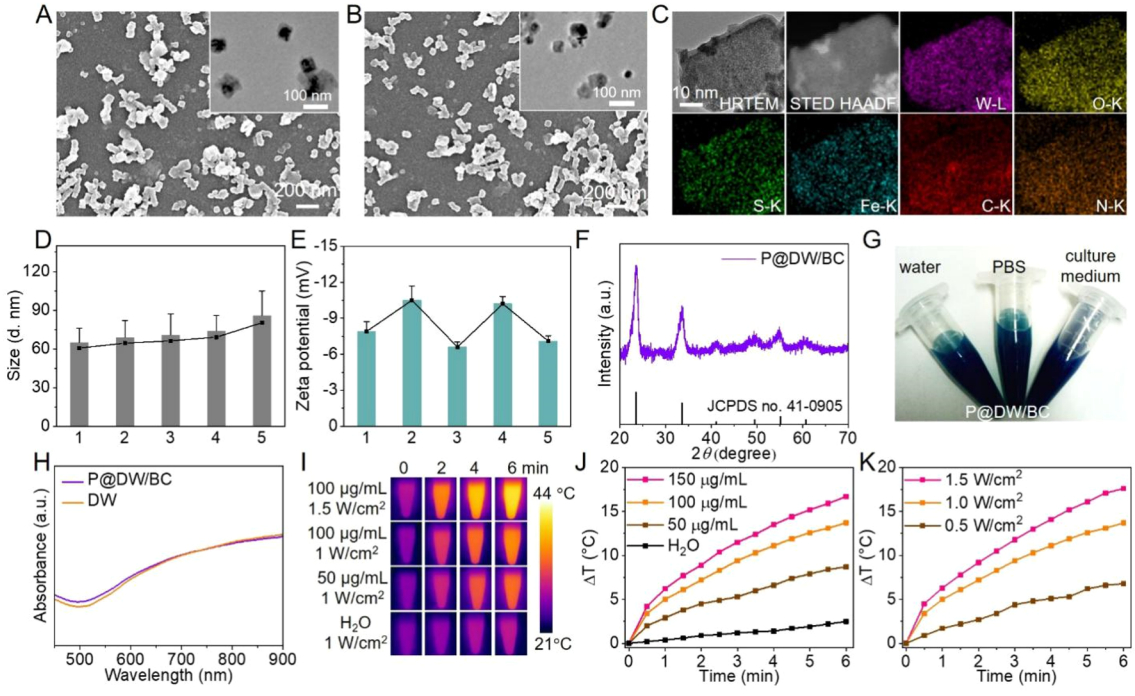

Figure 2. (A) SEM and TEM (inset) images of DW NSs. (B) SEM and TEM (inset) images of P@DW/BC NSs. (C) HRTEM image, STEM-HAAF image, and the corresponding element mapping images of P@DW/BC. (D) Hydrodynamic sizes and (E) ζ potentials of 1. DW NSs; 2. DW-PDA NSs; 3. DW/Fe^{3+} NSs; 4. DW/BC NSs; 5. P@DW/BC NSs. (F) PXRD pattern of P@DW/BC and JCPDS card of cubic WO_3. (G) Photographs of P@DW/BC NSs (1 mg mL^{-1}) dispersed in H_2O, PBS, and culture medium (containing 10% FBS). (H) UV−vis-NIR absorbance spectra of P@DW/BC NSs, DW NSs, and WO_3 atomic layers. (I) Thermal images of P@DW/BC solutions under 808 nm laser irradiation. (J) Heat curves of P@DW/BC solutions with various concentrations (Power density: 1 W cm^{-2}). (K) Heat curves of P@DW/BC solution (100 μg mL^{-1}) under 808 nm laser irradiation with different power densities.

https://dx.doi.org/10.1021/acscentsci.9b01342
ACS Cent. Sci. 2020, 6, 555−565

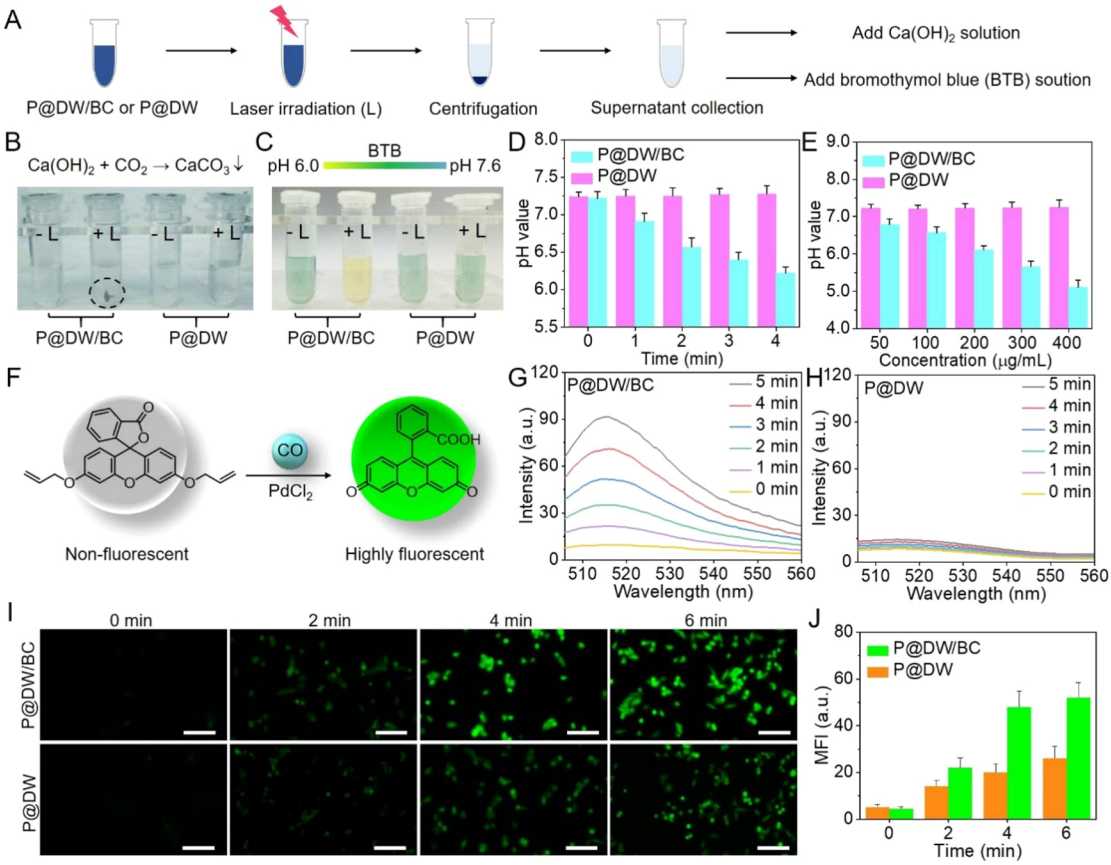

Figure 3. (A) Schematic of CO_2 detection via $Ca(OH)_2$ and pH change evaluation via BTB. (B) Chemical reaction of $CaCO_3$ formation (upper) and photographs of the samples after centrifugation. (C) The color change of BTB solution with pH change (up) and photographs of supernatants after the addition of BTB solution. (D) pH values of P@DW/BC and P@DW solutions (200 μg mL^{-1}) during 808 nm laser irradiation (1 W cm^{-2}). (E) pH values of P@DW/BC and P@DW solutions (50, 100, 200, 300, and 400 μg mL^{-1}) after 4 min of 808 nm laser irradiation (1 W cm^{-2}). (F) Schematic illustration of fluorescent detection of CO by the CO probe. Fluorescent spectra changes of (G) P@DW/BC and (H) P@DW solutions (100 μg mL^{-1}) together with CO probe and $PdCl_2$ under 808 nm laser irradiation (1 W cm^{-2}). (I) Fluorescent imaging of CO in CT26 cells after the treatment of P@DW/BC or P@DW (100 μg mL^{-1}) upon laser irradiation (1 W cm^{-2}). (J) Changes of the intracellular fluorescence intensity in (I).

Keeping all these in mind, here, a defective tungsten oxide (WO_3) (DW)-based NIR light responsive nanoreactor (termed as P@DW/BC) was fabricated for simultaneous tumor PTT and CO-mediated anti-inflammation. DW that was constructed by introducing oxygen vacancies higher than the reported critical density (7.3%) in WO_3 can result in an intermediate band and achieve infrared (IR) light-driven CO_2 splitting to produce CO,[21] making it an appealing material for *in vivo* CO generation. In addition, DW also possesses strong and broad absorbance ranging from NIR to IR region, which shows great potential to be extended as a PTA for tumor thermal ablation.[21] Moreover, bicarbonate (BC) was introduced to serve as a CO_2 releaser, which can quickly decompose into CO_2 upon heating to 40 °C or above.[22,23] As illustrated in Figure 1, DW nanosheets (DW NSs) were first decorated with lipoic acid conjugated dopamine (LA-DPA) through the W−S bonds. Then, ferric ion (Fe^{3+}) was introduced to serve as a coordination center to bridge both DPA and bicarbonate (BC), where Fe^{3+} can coordinate with the two − OH groups on DPA in a bidentate manner and with BC in a monodentate manner.[24,25] Finally, lipoic acid conjugated polyethylene glycol (LA-PEG) was engaged to improve the biocompatibility and dispersity of the nanosystem, thus providing PEG@DW/BC or P@DW/BC NSs. It was anticipated that after being injected intravenously, P@DW/BC could selectively accumulate in tumor tissues via the enhanced permeability and retention (EPR) effect. Then upon 808 nm laser irradiation, the DW content in P@DW/BC could conduct both photothermal conversion and CO_2 photoreduction to produce CO. Meanwhile, the generated heat was also supposed to trigger the decomposition of BC to produce CO_2 near the NSs, thus enhancing the CO generation by photocatalytic CO_2 reduction. Benefiting from the generated hyperthermia and CO upon single NIR laser irradiation, P@DW/BC was expected to effectively inhibit tumor growth by PTT and simultaneously weaken the PTT-induced inflammation by CO.

RESULTS AND DISCUSSION

DW atomic layers were first prepared by annealing WO_3 atomic layers in a reducing atmosphere to create oxygen vacancies according to the literature method (Figure S1).[21] Then the DW atomic layers were converted into DW NSs under sonication in water. Scanning electron microscopy (SEM) and transmission electron microscopy (TEM) images in Figure 2A clearly illustrated the uniform nanostructure of the as-prepared DW NSs. The powder X-ray diffraction (PXRD) pattern of DW NSs confirmed their crystal structure and all diffraction peaks can be indexed to cubic WO_3 (JCPDS

https://dx.doi.org/10.1021/acscentsci.9b01342
ACS Cent. Sci. 2020, 6, 555−565

no. 41-0905) (Figure S2).[26] Moreover, the O 1s X-ray photoelectron spectroscopy (XPS) spectrum in Figure S3 suggested the presence of abundant oxygen vacancies in DW Ns and the ratio of oxygen vacancies and oxygen atoms was calculated to be 14.7%, which was higher than the critical density of oxygen vacancies that is needed to realize IR-light-driven CO_2 reduction.[21] Then, LA-DPA was decorated on the surface of DW NSs via the W−S bonds to provide DW-DPA NSs.[27,28] The increased particle size (Figure 2D), decreased ζ potential (Figure 2E), and Fourier transform infrared spectroscopy (FTIR) spectra in Figure S4 revealed the successful preparation of DW-DPA NSs. After that, Fe^{3+} was introduced to coordinate with the two −OH groups on dopamine and also served as a bridge to coordinate with BC, thus providing DW/BC NSs. Compared with DW-PDA, a new peak of Fe 2p was observed in the XPS spectra in Figure S4, which indicated the successful introduction of Fe^{3+}. Finally, to improve the dispersion and biocompatibility of the material, LA-PEG was introduced to the NSs, which results in P@DW/BC NSs. As observed under SEM and TEM (Figure 2B), the as-prepared P@DW/BC NSs showed an average total size at about 65 nm. The elemental composition of P@DW/BC was revealed by MAPPING analysis, and the signals corresponding to W, O, S, Fe, C, and N were detected (Figure 2C). The W and Fe contents in P@DW/BC were detected to be 48 and 3.9 wt % via inductively coupled plasma-atomic emission spectroscopy (ICP-AES). Besides, the FTIR spectra of products (Figure S5) also confirmed the successful fabrication of P@DW/BC NSs. Importantly, the retained crystal structure of DW was revealed by PXRD analysis (Figure 2F), which indicated the modification process had a negligible influence on the crystalline phase of DW. The as-prepared P@DW/BC NSs exhibited a narrow hydrodynamic size at about 86 nm (PDI: 0.11) and a charge potential at about −7.1 eV, which were suitable for the EPR effect and long-term circulation of P@DW/BC NSs *in vivo*.[29,30] In addition, owing to the PEG modification, P@DW/BC NSs dispersed well in various physiological solutions including water, phosphate buffered saline (PBS, pH 7.4), and culture medium (RPMI 1640 containing 10% FBS) (Figure 2G). Both the size distribution and polydispersity index (PDI) of P@DW/BC NSs were almost constant in 7 days (PBS, pH 7.4) (Figure S6A). The TEM image in Figure S6B also revealed the good stability of P@DW/BC NSs under normal physiological conditions. Meanwhile, negligible Fe^{3+} (less than 6%) and CO_2 (less than 3%) release (Figure S7) were detected in 7 days (PBS, pH 7.4, 37 °C), indicating good stability of the Fe^{3+}-mediated coordination structure, which was consistent with the literature report.[24]

As shown in Figure 2H, the same as DW NSs, P@DW/BC NSs exhibited strong absorbance in the NIR region, indicating their good potential as efficient NIR-absorbing agents. In view of this, the photothermal conversion properties of P@DW/BC NSs were first studied. The temperature changes of P@DW/BC solutions under 808 nm laser irradiation were monitored by utilizing an IR camera. As shown in Figure 2I−K, the temperature of P@DW/BC solutions increased rapidly under irradiation, and the change depended closely on the concentration of P@DW/BC NSs as well as the power density of the NIR laser. These results clearly implied the great light-to-heat conversion ability of the as-prepared P@DW/BC NSs and also highlighted the controllability of heat generation. In particular, the photothermal conversion efficacy (η) of P@DW/BC NSs was calculated to be 39.1% (Figure S8), which was higher than or comparable to many of the reported PTAs (Table S1). Additionally, the photothermal effect of P@DW/BC NSs was almost unchanged during five irradiation OFF/ON cycles (Figure S9), confirming the good photothermal stability of P@DW/BC NSs.

Encouraged by the efficient photothermal conversion of P@DW/BC NSs, then the hyperthermia-induced CO_2 production ability of P@DW/BC NSs was studied. LA-PEG modified DW NSs (termed as P@DW NSs) that without the introduction of BC on the NSs were served as control material. As illustrated in Figure 3A, P@DW/BC and P@DW NSs (200 μg mL^{-1}) aqueous solutions were irradiated with/without 808 nm laser (1 W cm^{-2}, 4 min) and then centrifuged to obtain the supernatants. Afterward, calcium hydroxide ($Ca(OH)_2$) and bromothymol blue (BTB) solution were added to the supernatants for CO_2 detection and pH value evaluation, respectively. CO_2 was supposed to react with $Ca(OH)_2$ in water to yield $CaCO_3$ precipitation.[31] As shown in Figure 3B, whether P@DW/BC, P@DW, or P@D + Laser (L) group showed almost no precipitation after the addition of $Ca(OH)_2$. However, for P@DW/BC + L group, precipitation of $CaCO_3$ with gray-white color was clearly observed after the addition of $Ca(OH)_2$, demonstrating the successful generation of CO_2 by P@DW/BC under irradiation. Additionally, the release ratio of CO_2 was calculated to be 95% for P@DW/BC NSs after 4 min of laser irradiation, indicating the effective conversion of BC to CO_2 *in vitro*. Furthermore, considering that the generated CO_2 could dissolve in water, yielding carbonic acid to acidify the solution, acid−base indicator dye BTB was then utilized for the pH value evaluation of the supernatants. The color of the BTB solution would change from yellow to green and then to blue when the pH value of the solution increases from 6.0 to 7.0 and then to 7.6.[32] As shown in Figure 3C, after the addition of BTB, only the supernatant from P@DW/BC + L group showed a yellow color, while other three groups were green (the same color as BTB added to deionized water). This clearly indicated the relatively low pH value of supernatant from P@DW/BC + L group, further confirming the thermal-induced CO_2 release by P@DW/BC under irradiation. Additionally, the pH values of P@DW/BC and P@DW solutions after laser irradiation were also directly monitored by a pH meter. As displayed in Figure 3D, with the prolongation of the irradiation time, the pH value of P@DW/BC + L group decreased gradually, which revealed a dependence of the CO_2 producing amount on irradiation time. While for P@DW + L group, the pH value showed negligible change during the irradiation, indicating the lack of CO_2 production ability of P@DW NSs. Moreover, compared with P@DW + L group that increasing the concentration of the NSs had minimal effect on the pH value, P@DW/BC + L group exhibited an obvious pH value decrease with the increase of the concentration (Figure 3E), which provided strong evidence for the thermal-induced CO_2 release ability of P@DW/BC NSs.

Encouraged by the successful CO_2 generation by P@DW/BC NSs, whether the generated CO_2 would promote the photocatalytic CO production was then investigated. A literature reported fluorescent CO probe was utilized to monitor the CO generation. As illustrated in Figure 3F, the CO probe is nonfluorescent but exhibits a rapid and colorimetric fluorescent turn-on response for CO with the presence of $PdCl_2$, which can realize real-time and non-destructive CO detection.[33] P@DW/BC and P@DW NSs

https://dx.doi.org/10.1021/acscentsci.9b01342
ACS Cent. Sci. 2020, 6, 555−565

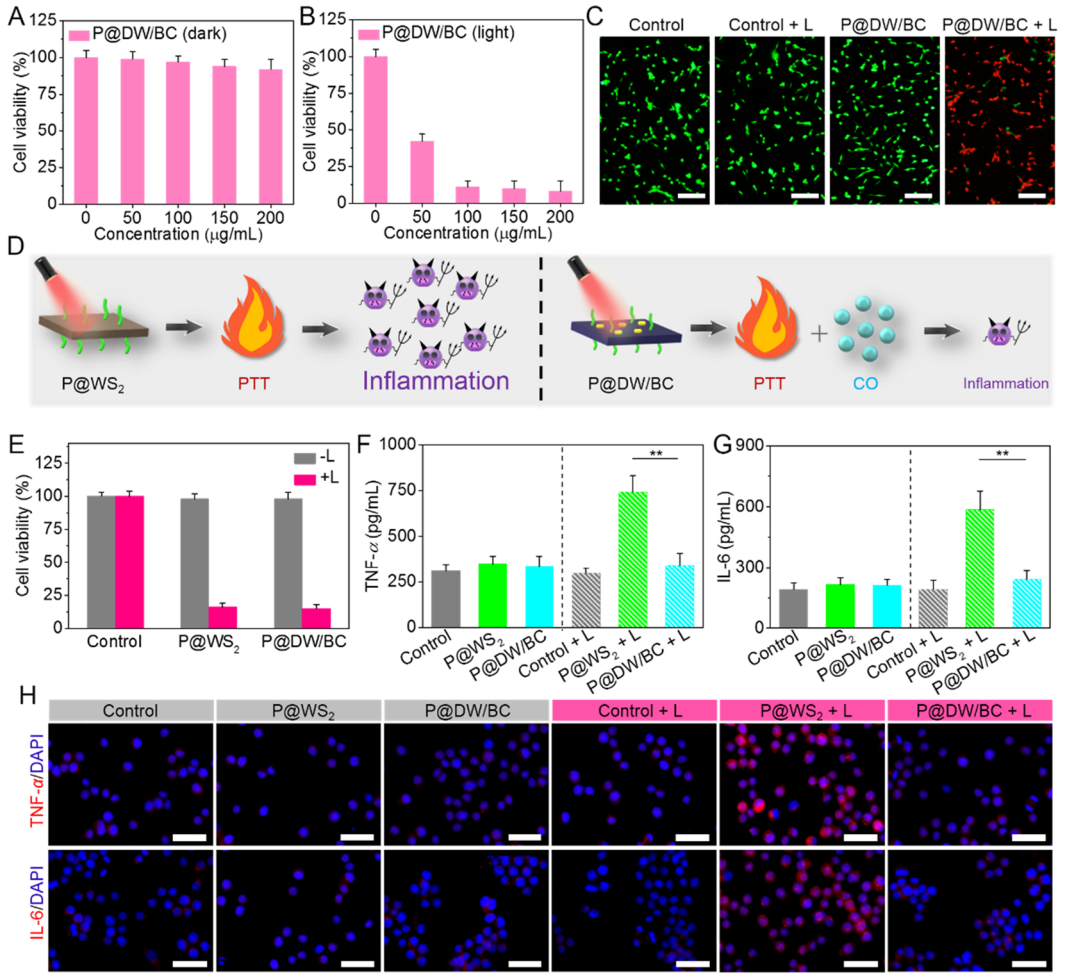

Figure 4. Cell viability of CT26 cells treated with P@DW/BC NSs with various concentrations (A) in the dark condition and (B) under 808 nm laser irradiation (1 W cm^{-2}, 6 min). (C) Live/dead staining images of CT26 cells after various treatments. Scale bar: 100 μm. Viable cells were stained green with calcein-AM, and dead/late apoptosis cells were stained red with PI. (D) Schematic of the different results after P@WS_2- or P@DW/BC NSs-mediated PTT. P@WS_2-mediated PTT was supposed to induce obvious inflammation, while the inflammatory reactions induced by P@DW/BC-mediated PTT was supposed to be largely reduced due to the generation of CO. (E) Cell viability of CT26 cells after various treatments. (F) TNF-α and (G) IL-6 levels of RAW 264.7 macrophages after treatment with media of different CT26 cell samples, $n = 3$, $^{**}p < 0.01$. (H) Representative immunofluorescence images of TNF-α and IL-6 expression in RAW 264.7 macrophages after treatment with media of different CT26 cell samples. Scale bar: 100 μm.

(100 μg mL^{-1}) were dispersed in water that boiled in advanced to remove the dissolved CO_2. Then CO probe and $PdCl_2$ were added and the mixtures were irradiated with 808 nm laser (1 W cm^{-2}). As displayed in Figure 3G, P@DW/BC solution showed distinct fluorescence enhancement in 5 min, demonstrating the effective CO generation upon laser irradiation. The conversion ratio of CO_2 to CO was detected to be 0.021%. However, for P@DW solution, negligible fluorescence enhancement was observed during the same period of laser irradiation (Figure 3H), which was owing to the insufficient CO_2 supply for the photocatalytic reaction. Furthermore, the CO generation abilities of P@DW/BC and P@DW NSs in living cells were also investigated. Mouse colon cancer (CT26) cells were coincubated with P@DW/BC or P@DW NSs in the same concentration (100 μg mL^{-1}) and then irradiated with 808 nm laser (1 W cm^{-2}). The intracellular CO generation was evaluated by using the same CO probe described above. As shown in Figure 3I, with the extension of the illustrating time, both P@DW/BC and P@DW NSs treated cells showed obvious fluorescence enhancement, indicating the successful CO generation in the cells. However, compared with P@DW that can only use the endogenous CO_2 for photocatalytic CO generation, P@DW/BC that can realize hyperthermia-induced CO_2 generation showed much stronger CO production ability in the cells. Specifically, the fluorescence intensity of P@DW/BC treated cells enhanced over 40 times after 6 min irradiation, which was significantly higher than that in P@DW treated ones (about 25 times) (Figure 3J). Such results fully demonstrated the successful CO generation by P@DW/BC NSs in living cells and also proved the effective enhancement of CO generation by the thermal-induced CO_2 release strategy.

Motivated by the good performance of P@DW/BC NSs above, then the cytotoxicity of P@DW/BC NSs was tested in CT26 cells. As shown in Figure 4A, no significant cytotoxicity was induced by P@DW/BC NSs at tested concentrations after 24 h, where the cell viabilities were still higher than 92% even the NSs concentrations were up to 200 μg mL^{-1}, suggesting the low toxicity of the P@DW/BC NSs in dark. In sharp contrast, cells after the treatment of P@DW/BC NSs upon 808 nm laser irradiation (1 W cm^{-2}, 6 min) were killed remarkably in which only less than 9% of the cells were still

https://dx.doi.org/10.1021/acscentsci.9b01342
ACS Cent. Sci. 2020, 6, 555−565

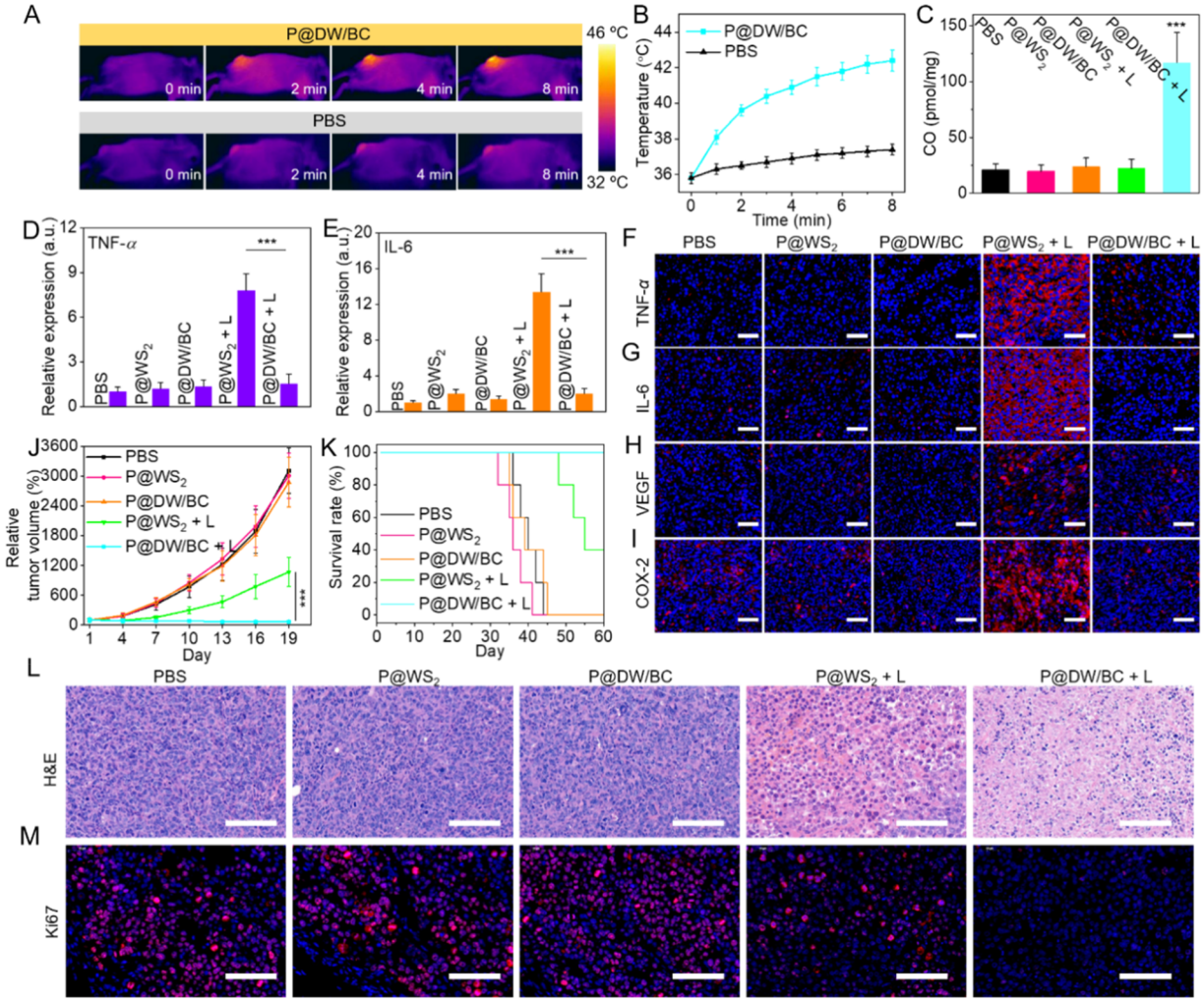

Figure 5. (A) *In vivo* IR thermal images of mice and (B) temperature increase curves of tumors after the treatments of PBS or P@DW/BC upon 808 nm laser irradiation (1 W cm^{-2}). (C) CO contents in tumor tissues of mice after various treatments. $n = 3$, $^{***}p < 0.001$. Relative expression of (D) TNF-α and (E) IL-6 in sera of mice at 24 h after various treatments, $n = 3$, $^{***}p < 0.001$. Representative immunofluorescence images for (F) TNF-α, (G) IL-6, (H) VEGF, and (I) COX-2 in tumor tissues of mice at 24 h after various treatments. Scale bar: 50 μm. (J) Relative tumor volume of mice during the experiments ($n = 6$). (K) Survival graph of mice from various groups ($n = 5$). Representative pictures of (L) H&E staining and (M) Ki67 immunofluorescence staining of tumor tissues of mice on the 19th day. Scale bar: 100 μm.

alive after 24 h (Figure 4B), suggesting the efficient tumor cells thermal ablation by P@DW/BC NSs. Additionally, the low cytotoxicity in the dark condition and good PTT effect of P@DW/BC NSs were also visually confirmed by live/dead cell staining assay as displayed in Figure 4C, which further proved the great potential of P@DW/BC NSs as safe and efficient PTAs for tumor PTT.

Furthermore, considering that P@DW/BC NSs can simultaneously achieve tumor PTT and CO generation under single 808 nm laser irradiation, whether the generated CO can effectively mitigate the inflammatory responses caused by PTT was investigated. Before that, previously reported PTAs, PEG conjugated tungsten sulfide (P@WS_2) NSs were prepared to serve as control material without CO generation ability (Figure S10).[34,35] As illustrated in Figure 4D, P@WS_2 NSs were supposed to effectively kill tumor cells via PTT but cause significant inflammatory reactions. While the inflammatory reactions caused by P@DW/BC-mediated PTT were expected to be largely reduced because of the presence of CO. To verify our conjecture, the inflammatory reactions after various treatments were evaluated by detecting the expression of pro-inflammatory cytokines tumor necrosis factor alpha (TNF-α) and interleukin-6 (IL-6) on RAW 264.7 macrophages.[36−38] As was expected, although the photothermal cytotoxicities of P@WS_2 and P@DW/BC were controlled basically the same (Figure 4E), the inflammatory reactions after the treatments were quite different. The treatment of laser irradiation, P@WS_2, or P@DW/BC exhibited negligible effect on the secretion of TNF-α and IL-6 (Figure 4F,G), indicating these treatments would induce negligible inflammatory responses. However, the secretion of TNF-α and IL-6 were dramatically increased after the treatment of P@WS_2 + L, indicating the remarkable pro-inflammatory responses caused by PTT. On the contrary, the expression levels of TNF-α and IL-6 were minimally affected by P@DW/BC + L, suggesting the inflammatory responses caused by PTT were effectively inhibited. Apart from these, immunocytochemistry staining was also performed to visualize the expression levels of TNF-α and IL-6 in macrophages. As shown in Figure 4H, compared with P@WS_2 + L group that induced obvious overproduction of TNF-α and IL-6, the treatment of P@DW/BC + L exhibited limited effect on the expression of TNF-α and IL-6,

https://dx.doi.org/10.1021/acscentsci.9b01342
ACS Cent. Sci. 2020, 6, 555−565

which further verified that the CO generated by P@DW/BC can effectively eliminate the inflammation triggered by PTT.

After confirming the feasibility of P@DW/BC NSs for *in vitro* PTT and anti-inflammation, the possibility of P@DW/BC NSs for *in vivo* applications was then investigated. CT26 xenograft BALB/c mice were used as animal models for the assessments. Cy5.5-labeled P@DW/BC NSs were first prepared and injected intravenously to mice to investigate the biodistribution of the NSs *in vivo* using a small animal imaging system. It can be seen that the fluorescence signal at tumor tissue increased gradually in the first 12 h and kept at a high level even at 24 h after the injection (Figure S11). This clearly demonstrated the selective accumulation of P@DW/BC in tumor tissue and 12 h post injection was chosen as the appropriate time point for laser irradiation. As shown in Figure 5A,B, the temperature of tumor area increased remarkably to over 42 °C after 8 min of 808 nm laser illustration (1 W cm^{-2}), which was capable of ablating tumor cells by moderate hyperthermia. In marked contrast, the tumor temperature of mice injected with PBS just increased by less than 2 °C after the same irradiation. These results confirmed that P@DW/BC NSs can be effective agents for *in vivo* tumor PTT.

Then, the CO content in tumor tissues after various treatments were also monitored.[20] It can be seen that the treatment of P@WS_2, P@WS_2 + L, or P@DW/BC alone minimally affected the CO content in tumor (Figure 5C). However, for mice treated with P@DW/BC + L, the CO content in tumor increased remarkably and was detected to be nearly 6 times as high as that in PBS group. This fully demonstrated the successful CO generation by P@DW/BC NSs under 808 nm laser irradiation *in vivo*. Notably, P@DW/BC NSs also exhibited better CO generation ability than P@DW NSs *in vivo* (Figure S12), proving that the thermal-induced CO_2 release strategy can also promote *in vivo* CO generation.

Furthermore, whether the CO generated by P@DW/BC NSs can effectively reduce the PTT triggered inflammation was studied. The levels of the cytokines in sera of mice after various treatments were first evaluated. As shown in Figure 5D,E, the treatment of P@WS_2 or P@DW/BC alone showed minimal effect on the cytokine levels of TNF-α and IL-6 in sera of mice, indicating both of them induced negligible pro-inflammatory responses. However, after the treatment of P@WS_2 + L, the levels of TNF-α and IL-6 in sera of mice increased obviously, which was attributed to the inflammatory responses caused by PTT. In striking contrast, the levels of TNF-α and IL-6 in sera of P@DW/BC + L group showed no significant difference when compared with that of the PBS group, suggesting the superior anti-inflammation effect of CO. In addition, the expression of TNF-α and IL-6 in tumor tissues after the treatments was also investigated by immunofluorescence staining. Figure 5F,G show that P@DW/BC + L induced much lower expression of TNF-α and IL-6 in tumor tissue when compared with P@WS_2 + L, which verified the good anti-inflammatory effect of CO. Moreover, the expression of vascular endothelial growth factor (VEGF) and cyclooxygenase-2 (COX-2) in tumor tissues after various treatments were also investigated. The inflammatory responses are supposed to trigger the expression of them, which could diminish the therapeutic efficacy and create enhanced environment for tumor recurrence.[39,40] It can be seen that different from PTT alone (P@WS_2 + L) that triggered the promotion of VEGF and COX-2 in tumor, the combination of PTT with CO (P@DW/BC + L) resulted in largely weakened expression of them in tumor (Figure 5H,I), which clearly demonstrated that the CO-mediated anti-inflammation was beneficial for effective tumor therapy.

Afterward, the *in vivo* antitumor efficacy of the samples was studied. CT26-tumor-bearing mice were randomly divided into five groups and treated with PBS, P@WS_2 (100 μL, 9 mg mL^{-1}), P@DW/BC (100 μL, 10 mg mL^{-1}), P@WS_2 + L (1 W cm^{-2}, 8 min), and P@DW/BC + L, respectively. It should be pointed out that the dosage of P@WS_2 NSs injected to mice can achieve nearly the same photothermal effect as P@DW/BC NSs *in vivo* (Figure S13). As shown in Figure 5J, the treatment of P@DW/BC or P@WS_2 NSs alone showed nearly no effect on tumor suppression. Although both the treatments of P@DW/BC + L and P@WS_2 + L obviously inhibited the tumor growth at the beginning (almost the first 4 days), the tumor volume in P@WS_2 + L group increased rapidly after 1 week while the tumor volume in P@DW/BC + L group kept nearly unchanged even after 19 days. Specifically, the tumor inhibition rate of P@DW/BC + L group reached over 96% and was obviously higher than that of P@WS_2 + L group (74%) at the end point of the experiment (Day 19). Moreover, the tumor tissues of mice after various treatments were also collected for hematoxylin-eosin (H&E) staining and Ki67 immunofluorescence staining fluorescence. The results in Figure 5L,M showed that the treatment of P@DW/BC + L triggered much stronger cellular damage and resulted in much weaker cell proliferation when compared with P@WS_2 + L, further validating the synergistic effect of CO and PTT for tumor inhibition. Importantly, CO-mediated anti-inflammation also greatly improved the survival rate of mice after PTT. It was found that over 60% of mice died in the P@WS_2 + L group, while 100% of the mice in P@DW/BC + L group were still alive after 60 days (Figure 5K), demonstrating the combination of CO with PTT was also beneficial for the long-term treatment of tumors.

Moreover, the potential systemic toxicity of P@DW/BC was evaluated. No abnormal body changes of mice were observed during the treatment (Figure S14). Meanwhile, blood biochemistry analysis (Figure S15) and H&E staining of major organs (Figure S16) of mice on the 19th day also suggested that no acute side effect was caused after the treatment. Both of these indicated the good biosafety of P@DW/BC NSs *in vivo*.

CONCLUSIONS

In summary, an NIR laser responsive nanoreactor P@DW/BC was fabricated for simultaneous tumor PTT and anti-inflammation. Upon single 808 nm laser irradiation, P@DW/BC can realize both photothermal conversion and CO_2 photoreduction to produce CO. Moreover, the heat triggered by P@DW/BC can also lead to the decomposition of BC to produce CO_2 near the nanoreactor, thus enhancing the CO generation under laser irradiation. Owing to the good photothermal effect and CO generation *in vivo*, P@DW/BC can effectively suppress tumor growth and also reduce the inflammatory responses caused by PTT, which showed great therapeutic advantages compared with traditional PTAs. We hope that this study could provide new ideas for the application of CO in biomedical fields and also point out new directions for the combination of PTT and anti-inflammation therapy.

https://dx.doi.org/10.1021/acscentsci.9b01342
ACS Cent. Sci. 2020, 6, 555−565

MATERIALS AND METHODS

Materials. Tungsten chloride (WCl_6) and oxalic acid (OA) were purchased from Adamas Reagent Co., Ltd. (Shanghai, China). LA-PEG (M_w = 5000) was obtained from Ponsure Biotech, Inc. (Shanghai, China). α-Lipoic acid and dopamine hydrochloride were acquired from Alfa Aesar chemical company (China). Cy5.5-PEG-SH (M_w = 2000) was provided by Shanghai ToYongBio Tech.Inc. (China). Ferric chloride·$6H_2O$ ($FeCl_3 \cdot 6H_2O$) and ammonium bicarbonate (NH_4HCO_3) were purchased from Sinopharm Group Co., Ltd. Roswell Park Memorial Institute (RPMI) 1640 medium, fetal bovine serum (FBS), penicillin−streptomycin, and trypsin were obtained from BI Corp. Calcein-AM and propidium iodide were obtained from 4A Biotech Co., Ltd. (Beijing, China). 3-[4,5-Dimethylthiazol-2-yl]-2,5-diphenyltetrazolium bromide (MTT) was purchased from Thermo Fisher (China). Bulk tungsten disulfide (WS_2, 99.9%, 2 μm) was supplied by Aladdin Reagent (Shanghai, China). TNF-α and IL-6 ELISA kits were purchased from 4A Biotech Co., Ltd. (Beijing, China). Carbon monoxide assay kit (A101-2) was obtained from Nanjing Jiancheng Bioengineering Institute (China). All other reagents and solvents were used without further purification.

Instrumentation. Morphological observation was performed under transmission electron microscopy (TEM, JEOL-2100 Japan). Zeta potential and hydrodynamic diameter were measured by dynamic light scattering (DLS) on a Zetasizer ZEN3600 (Malvern). FTIR was collected on a PerkinElmer spectrophotometer. UV−vis-NIR spectra were collected by UV−vis-NIR spectrophotometry Lambda 35 (PerkinElmer). XPS analysis was carried out on an ESCALAB 250XI (Thermo Fisher Scientific) at Shiyanjia club. PXRD analysis was performed by Rigaku MiniFlex 600 X-ray diffractometer (Cu Kα, λ = 1.5418 Å). The *in vivo* imaging experiments were studied using IVIS imaging systems (PerkinElmer). An 808 nm NIR laser (STL808T1−7.0 W) was purchased from Beijing STONE Laser.

Preparation of Defective WO_3 (DW) Atomic Layers. DW atomic layers were prepared by annealing WO_3 atomic layers in a reducing atmosphere. Briefly, WCl_6 (0.5 g) and OA (5 g) were dissolved in 100 mL of ethanol. After the mixture was stirred for 0.5 h, it was transferred into a Teflon-lined autoclave, maintained at 100 °C for 24 h, and then cooled to room temperature. The product was washed with DI water and ethanol for 5 times, respectively, and vacuum-dried overnight at 60 °C to obtain WO_3 atomic layers with a yellow color. Finally, the as-prepared WO_3 atomic layers were calcined under a mixed gas (20% H_2/Ar) at 300 °C for 1 h (heating rate: 10 °C/min) to provide DW atomic layers with dark blue color.

Preparation of LA-PDA. LA-DPA was synthesized according to the literature report. Triethylamine (0.1 g) was added to 20 mL of ethanol which contains dopamine hydrochloride (0.19 g) under N_2. The mixture was stirred at room temperature for 1 h and followed by the addition of α-lipoic acid (0.2 g) and EEDQ (0.25 g). After stirring at room temperature for 24 h under N_2, the mixture was filtered. The filter was evaporated and purified by column chromatography on silica gel to provide LA-DPA (0.18 g, yield: 53%). The obtained LA-DPA was characterized by ESI-MS: m/z calculated: 341.1, found: 340.1 $[M-H]^-$.

Preparation of DW NSs. DW atomic layers (50 mg) were dispersed in 30 mL of DI water for untrasonication for 2 h in an ice-bath. Then the mixture was centrifugated in 3000 rpm to move the large particles, thus providing DW NSs.

Preparation of P@DW/BC NSs. DW NSs aqueous solution (1 mg mL^{-1}, 20 mL) was added by LA-DPA (10 mg) and then stirred at room temperature for 6 h. After that, the mixture was centrifugated and washed with DI water and ethanol. The as-prepared DW-PDA NSs were then dispersed in ethanol. Next, $FeCl_3 \cdot 6H_2O$ (10 mg) was added to the DW-PDA ethanol solution, and the mixture was stirred overnight. Afterward, the mixture was centrifugated and washed with DI water and ethanol to obtain Fe^{3+} modified DW Fe^{3+} NSs. Subsequently, 1 mL of NH_4HCO_3 solution (5 mM) was added to the DW Fe^{3+} ethanol solution every 1 h under ice-bath, followed by 5 additions. Then, the products were centrifugated and washed with ice water to obtain DW/BC NSs. Moreover, LA-PEG (15 mg) was added to the DW/BC aqueous solution and the mixture was stirred at an ice-bath for 6 h. Finally, the mixture was washed with DI water to remove the excess LA-PEG, thus providing P@DW/BC NSs.

Preparation of P@WS_2 NSs. Bulk WS_2 (20 mg, 99.9%, 2 μm) was dispersed in 30 mL of water for untrasonication for 6 h in an ice-bath. Then the mixture was centrifugated and washed with DI water to obtain WS_2 NSs. For PEG modification, 10 mg of WS_2 NSs was mixed with 10 mg of LA-PEG in 30 mL of water. After the mixture was stirred at room temperature for 6 h, excess LA-PEG was removed by centrifugation and repeated water washing, thus obtaining PEG@WS_2 NSs with a hydrodynamic size of about 72 nm.

***In Vitro* Photothermal Effect.** P@DW/BC NSs aqueous solution (1 mL) with various concentrations (0, 50, 100, and 150 μg mL^{-1}) were irradiated with 808 nm laser (0.5, 1, or 1.5 W cm^{-2}). The temperature of the solution was recorded by an IR camera during the irradiation.

CO_2 Detection via $Ca(OH)_2$ and pH Value Evaluation via BTB. DI water was boiled in advance to remove the naturally dissolved CO_2. Then P@DW/BC or P@DW NSs (400 μg) were dispersed in the water, irradiated with 808 nm laser (1 W cm^{-2}, 4 min) and centrifugated (10 000 rpm, 15 min) at 25 °C. The supernatants were collected and added by 0.5 mL of $Ca(OH)_2$ aqueous solution (1 mg mL^{-1}). Finally, the mixture was centrifugated (3000 rpm, 5 min) to determine whether $CaCO_3$ precipitation was yield. For pH value evaluation via BTB, to the supernatants that were collected above was added BTB, and then photos of the mixtures were taken.

***In Vitro* CO Detection.** For *in vitro* CO detection, 1 mL of P@DW/BC or P@DW NSs (100 μg mL^{-1}) aqueous solution (in which the water was boiled in advance) were added by CO probe (5 μM) and $PdCl_2$ (5 μM). The mixtures were then irradiated with 808 nm laser (1 W cm^{-2}) for 5 min. The fluorescent spectra of the mixtures were recorded (Ex: 490 nm).

Cell Culture. CT26 cells were cultured in 1640 medium containing 1% antibiotics (penicillin-streptomycin, 10 000 U/mL) and 10% FBS. Macrophages (RAW 264.7) were cultured in DMEM medium containing 1% antibiotics (penicillin-streptomycin, 10 000 U/mL) and 10% FBS. These cells were grown at 37 °C with 5% CO_2 in a humidified atmosphere.

Intracellular CO Detection. For intracellular CO detection, CT26 cells were incubated with P@DW/BC or P@DW NSs (100 μg mL^{-1}) for 4 h. Then the culture medium

https://dx.doi.org/10.1021/acscentsci.9b01342
ACS Cent. Sci. 2020, 6, 555−565

was replaced by the fresh medium, and cells were irradiated with a 808 nm laser for 0, 2, 4, or 6 min. Finally, cells were coincubated with a mixture of CO probe (1 μM) and $PbCl_2$ (1 μM) for 30 min, washed with PBS, and then observed via CLSM.

Cytotoxicity and Live/Dead Cell Staining Assay. CT26 cells were coincubated with P@DW/BC NSs with various concentrations for 4 h. Then the culture medium was replaced by new medium. Cells were irradiated with/without 808 nm laser (1 W cm^{-2}) for 6 min and then further cultured for 20 h. Afterward, MTT (20 μL, 5 mg mL^{-1}) was added to each well, and cells were further coincubated for 4 h. Finally, the supernatant was replaced by 150 μL of DMSO and shaken well to measure the optical density (OD). The cell viability was determined by the following formula: cell viability (%) = $OD_{(sample)}/OD_{(control)} \times 100\%$. For the live/dead staining assay, cells were stained at 4 h post irradiation with calcein-AM and PI for 15 min and then observed by an inverted microscope.

Determination of Cell Cytokine Production. CT26 cells were coincubated with P@DW/BC or P@WS_2 NSs for 4 h. Then the culture medium was replaced by new medium, and cells were irradiated with 808 nm laser (1 W cm^{-2}, 6 min). After that, the supernatants of the CT26 cells were transferred to the culture medium of macrophages, and the macrophages were incubated overnight. The supernatants of the macrophages were collected and analyzed using ELISA kits to evaluate the levels of TNF-α and IL-6. Besides, the macrophages that were incubated overnight were also collected, washed with PBS, fixed with 4% formaldehyde, and followed by the evaluation of the levels of intracellular expression of TNF-α and IL-6 via immunocytochemistry staining.

Animal and Tumor Models. The animal experiments were performed according to the guidelines for laboratory animals established by the Wuhan University Center for Animal Center Experiment/A3-Lab, and all study protocols were subject to approval by the Institutional Center of Wuhan University (Wuhan, China). Six-week-old female BALB/c mice were subcutaneously injected with 100 μL of CT26 cells suspension ($\sim 10^7$) per mouse on the right back of the hind leg. Mice were used for *in vivo* photothermal imaging and antitumor study when the tumor size reached about 100 mm^3.

***In Vivo* Biodistribution of P@DW/BC NSs.** First, Cy5.5-modified P@DW/BC NSs were prepared by mixing Cy5.5-PEG-SH with P@DW/BC (w/w = 1/50) in PBS (pH = 7.4) for 4 h. Then the mixture was washed with PBS and centrifugated to remove the excess Cy5.5-PEG-SH, thus providing Cy5.5-modified P@DW/BC NSs. For *in vivo* imaging, CT26-tumor-bearing mice were intravenously injected with 100 μL of the prepared Cy5.5-modified P@DW/BC NSs and imaged by the small animal imaging system (IVIS Spectrum). At 24 h post injection, mice were sacrificed, and the tumor and major organs were collected for *ex vivo* imaging to evaluate the biodistribution of the NSs.

***In Vivo* Photothermal Imaging.** CT26-tumor-bearing mice were intravenously injected with 100 μL of PBS or P@DW/BC (10 mg mL^{-1}). Twelve hours later, the tumors of mice were irradiated with 808 nm laser (1 W cm^{-2}, 8 min), and the temperatures of mice were recorded by an IR camera during the irradiation.

CO Detection in Tumor Tissues. CT26-tumor-bearing mice were intravenously injected PBS, P@DW/BC (100 μL, 10 mg mL^{-1}), or P@WS_2 (100 μL, 9 mg mL^{-1}). Then 808 nm laser (1 W cm^{-2}, 8 min) was given at tumor regions at 12 h post injection. After that, the tumor tissues of mice were quickly collected for CO detection using an endogenous CO assay kit.

***In Vivo* Anti-Tumor Studies.** CT26 tumor-bearing mice were randomly divided into 5 groups (PBS, P@WS_2, P@DW/BC, P@WS_2 + L, and P@DW/BC + L). P@DW/BC (100 μL, 10 mg mL^{-1}) and P@WS_2 (100 μL, 9 mg mL^{-1}) were intravenously injected to mice on the first day. An 808 nm laser (1 W cm^{-2}, 8 min) was given at 12 h post injection. The tumor volumes and body weights of mice were recorded every 4 days. The tumor volume was calculated as $V = 1/2 \times (\text{tumor length}) \times (\text{tumor width})^2$, and the relative tumor volume was defined as V/V_0 (V_0 was the tumor volume that the treatment was initiated). The relative body weight was defined as W/W_0 (W_0 was the body weight that the treatment was initiated). On day 19, the mice from different groups were randomly selected and then dissected. The major organs (hearts, livers, spleens, lungs, and kidneys) and tumor tissues were collected for H&E staining. Moreover, the tumor tissues were also collected for Ki67 staining to evaluate the tumor cell proliferation. For the survival test, the remaining mice in each group (n = 5) were observed every day to determinate the survival percentage and euthanized on day 60.

***In Vivo* Anti-Inflammation Studies.** Serum samples were isolated from mice after various treatments at 24 h. Then the expression levels of TNF-α and IL-6 were analyzed using ELISA kits. Moreover, the tumor tissues of mice after various treatments at 24 h were also collected for immunocytochemistry staining to determine the expression of TNF-α, IL-6, VEGF, and COX-2.

Systemic Toxicity Evaluation. On the 19th day, the blood samples of mice were collected for blood biochemistry analysis.

Statistical Analysis. Statistical analysis was performed using a two-tailed Student's t test. All data were presented as means ± standard deviation (SD). The differences were considered to be statistically significant for a p value <0.05 ($^*p < 0.05$, $^{**}p < 0.01$, $^{***}p < 0.001$).

■ ASSOCIATED CONTENT

Supporting Information

The Supporting Information is available free of charge at https://pubs.acs.org/doi/10.1021/acscentsci.9b01342.

Preparation of DW nanosheets and other supporting figures and tables (PDF)

■ AUTHOR INFORMATION

Corresponding Author

Xian-Zheng Zhang − *Key Laboratory of Biomedical Polymers of Ministry of Education & Department of Chemistry and Institute for Advanced Studies (IAS), Wuhan University, Wuhan 430072, P. R. China;* orcid.org/0000-0001-6242-6005; Email: xz-zhang@whu.edu.cn

Authors

Shi-Bo Wang − *Key Laboratory of Biomedical Polymers of Ministry of Education & Department of Chemistry and Institute for Advanced Studies (IAS), Wuhan University, Wuhan 430072, P. R. China*

https://dx.doi.org/10.1021/acscentsci.9b01342
ACS Cent. Sci. 2020, 6, 555−565

Cheng Zhang − *Key Laboratory of Biomedical Polymers of Ministry of Education & Department of Chemistry, Wuhan University, Wuhan 430072, P. R. China*

Jing-Jie Ye − *Key Laboratory of Biomedical Polymers of Ministry of Education & Department of Chemistry, Wuhan University, Wuhan 430072, P. R. China*

Mei-Zhen Zou − *Key Laboratory of Biomedical Polymers of Ministry of Education & Department of Chemistry and Institute for Advanced Studies (IAS), Wuhan University, Wuhan 430072, P. R. China*

Chuan-Jun Liu − *Key Laboratory of Biomedical Polymers of Ministry of Education & Department of Chemistry, Wuhan University, Wuhan 430072, P. R. China;* orcid.org/0000-0001-9543-7763

Complete contact information is available at: https://pubs.acs.org/10.1021/acscentsci.9b01342

Author Contributions

#S.-B.W. and C.Z. contributed equally.

Notes

The authors declare no competing financial interest.

■ ACKNOWLEDGMENTS

We gratefully acknowledge financial support from the National Natural Science Foundation of China (51833007, 21674084, and 51690152). The CO probe was kindly provided by Dr. Shu-Min Feng (College of Chemistry, Central China Normal University, Wuhan, China).

■ REFERENCES

(1) Dickerson, E. B.; Dreaden, E. C.; Huang, X. H.; El-Sayed, I. H.; Chu, H. B.; Pushpanketh, S.; McDonald, J. F.; El-Sayed, M. A. Gold Nanorod Assisted Near-Infrared Plasmonic Photothermal Therapy (PPTT) of Squamous Cell Carcinoma in Mice. *Cancer Lett.* **2008**, *269*, 57−66.

(2) Cheng, L.; Wang, C.; Feng, L. Z.; Yang, K.; Liu, Z. Functional Nanomaterials for Phototherapies of Cancer. *Chem. Rev.* **2014**, *114*, 10869−10939.

(3) Shao, J. D.; Xie, H. H.; Huang, H.; Li, Z. B.; Sun, Z. B.; Xu, Y. H.; Xiao, Q. L.; Yu, X. F.; Zhao, Y. T.; Zhang, H.; Wang, H. Y.; Chu, P. K. Biodegradable Black Phosphorus-Based Nanospheres for *In vivo* Photothermal Cancer Therapy. *Nat. Commun.* **2016**, *7*, 12967.

(4) Yang, K.; Zhang, S.; Zhang, G. X.; Sun, X. M.; Lee, S. T.; Liu, Z. Graphene in Mice: Ultrahigh *In vivo* Tumor Uptake and Efficient Photothermal Therapy. *Nano Lett.* **2010**, *10*, 3318−3323.

(5) Lal, S.; Clare, S. E.; Halas, N. J. Nanoshell-Enabled Photothermal Cancer Therapy: Impending Clinical Impact. *Acc. Chem. Res.* **2008**, *41*, 1842−1851.

(6) Ray, P. C.; Khan, S. A.; Singh, A. K.; Senapati, D.; Fan, Z. Nanomaterials for Targeted Detection and Photothermal Killing of Bacteria. *Chem. Soc. Rev.* **2012**, *41*, 3193−3209.

(7) Okuno, T.; Kato, S.; Hatakeyama, Y.; Okajima, J.; Maruyama, S.; Sakamoto, M.; Mori, S.; Kodama, T. Photothermal Therapy of Tumors in Lymph Nodes Using Gold Nanorods and Near-Infrared Laser Light. *J. Controlled Release* **2013**, *172*, 879−884.

(8) Philip, M.; Rowley, D. A.; Schreiber, H. Inflammation as A Tumor Promoter in Cancer Induction. *Semin. Cancer Biol.* **2004**, *14*, 433−439.

(9) Mantovani, A. Cancer: Inflaming Metastasis. *Nature* **2009**, *457*, 36−37.

(10) Solinas, G.; Marchesi, F.; Garlanda, C.; Mantovani, A.; Allavena, P. Inflammation-Mediated Promotion of Invasion and Metastasis. *Cancer Metastasis Rev.* **2010**, *29*, 243−248.

(11) Coussens, L. M.; Zitvogel, L.; Palucka, A. K. Neutralizing Tumor-Promoting Chronic Inflammation: A Magic Bullet? *Science* **2013**, *339*, 286−291.

(12) Li, Y. J.; Dang, J. J.; Liang, Q. J.; Yin, L. C. Thermal-Responsive Carbon Monoxide (CO) Delivery Expedites Metabolic Exhaustion of Cance Cells toward Reversal of Chemotherapy Resistance. *ACS Cent. Sci.* **2019**, *5*, 1044−1058.

(13) Zuckerbraun, B. S.; Chin, B. Y.; Wegiel, B.; Billiar, T. R.; Czsimadia, E.; Rao, J.; Shimoda, L.; Ifedigbo, E.; Kanno, S.; Otterbein, L. E. Carbon Monoxide Reverses Established Pulmonary Hypertension. *J. Exp. Med.* **2006**, *203*, 2109−2119.

(14) Wareham, L. K.; Poole, R. K.; Tinajero-Trejo, M. CO-Releasing Metal Carbonyl Compounds as Antimicrobial Agents in the Post-Antibiotic Era. *J. Biol. Chem.* **2015**, *290*, 18999−19007.

(15) Motterlini, R.; Otterbein, L. E. The Therapeutic Potential of Carbon Monoxide. *Nat. Rev. Drug Discovery* **2010**, *9*, 728−743.

(16) Otterbein, L. E.; Bach, F. H.; Alam, J.; Soares, M.; Tao Lu, H.; Wysk, M.; Davis, R. J.; Flavell, R. A.; Choi, A. M. Carbon Monoxide Has Anti-Inflammatory Effects Involving the Mitogen-Activated Protein Kinase Pathway. *Nat. Med.* **2000**, *6*, 422−428.

(17) Katada, K.; Bihari, A.; Mizuguchi, S.; Yoshida, N.; Yoshikawa, T.; Fraser, D. D.; Potter, R. F.; Cepinskas, G. Carbon Monoxide Liberated from CO-Releasing Molecule (CORM-2) Attenuates Ischemia/Reperfusion (I/R)-Induced Inflammation in the Small Intestine. *Inflammation* **2010**, *33*, 92−100.

(18) Ji, X. Y.; Zhou, C.; Ji, K. L.; Aghoghovbia, R. E.; Pan, Z. X.; Chittavong, V.; Ke, B. W.; Wang, B. H. Click and Release: A chemical Strategy toward Developing Gasotransmitter Prodrugs by Using An Intramolecular Diels-Alder Reaction. *Angew. Chem., Int. Ed.* **2016**, *55*, 15846−15851.

(19) Zheng, D. W.; Li, B.; Li, C. X.; Xu, L.; Fan, J. X.; Lei, Q.; Zhang, X.-Z. Photocatalyzing CO_2 to CO for Enhanced Cancer Therapy. Zhang, X. Z. *Adv. Mater.* **2017**, *29*, 1703822.

(20) Wang, S. B.; Zhang, C.; Chen, Z. X.; Ye, J. J.; Peng, S. Y.; Rong, L.; Liu, C. J.; Zhang, X. Z. A versatile Carbon Monoxide Nanogenerator for Enhanced Tumor Therapy and Anti-Inflammation. *ACS Nano* **2019**, *13*, 5523−5532.

(21) Liang, L.; Li, X. D.; Sun, Y. F.; Tan, Y. L.; Jiao, X. C.; Ju, H. X.; Qi, Z. M.; Zhu, J. F.; Xie, Y. Infrared Light-Driven CO^2 Overall Splitting at Room Temperature. *Joule* **2018**, *2*, 1004−1016.

(22) Chung, M. F.; Chen, K. J.; Liang, H. F.; Liao, Z. X.; Chia, W. T.; Xia, Y. N.; Sung, H. W. A Liposomal System Capable of Generating CO^2 Bubbles to Induce Transient Cavitation, Lysosomal Rupturing, and Cell ecrosis. *Angew. Chem., Int. Ed.* **2012**, *51*, 10089.

(23) Nam, Y. S.; Yoon, J. J.; Park, T. G. A Novel Fabrication Method of Macroporous Biodegradable Polymer Scaffolds Using Gas Foaming Salt as A Porogen Additive. *J. Biomed. Mater. Res.* **2000**, *53*, 1−7.

(24) Li, W. P.; Su, C. H.; Wang, S. J.; Tsai, F. J.; Chang, C. T.; Liao, M. C.; Yu, C. C.; Vi Tran, T.- T.; Lee, C. N.; Chiu, W. T.; Wong, T. W.; Yeh, C. S. CO_2 Delivery to Accelerate Incisional Wound Healing Following Single Irradiation of Near-Infrared Lamp on the Coordinated Colloids. *ACS Nano* **2017**, *11*, 5826−5835.

(25) Chen, L. X.; Liu, T.; Thurnauer, M. C.; Csencsits, R.; Rajh, T. Fe_2O_3 Nanoparticle Structure Investigated by X-Ray Absorption Near-Edge Struture, Surface Modifcation, and Model Calculations. *J. Phys. Chem. B* **2002**, *106*, 8539−8546.

(26) Varghese, K. G.; Vaidyan, V. K. Phase Transition Studies of WO_3 Nanoparticles by XRD and FT Raman Spectroscopy. *AIP Conf. Proc.* **2008**, *1075*, 121−124.

(27) Zhi, L. H.; Zhang, H. L.; Yang, Z. Y.; Liu, W. S.; Wang, B. D. Inferface Coassembly of Mesoporous MoS_2 Based-Frameworks for Enhanced Near-Infrared Light Driven Photocatalysis. *Chem. Commun.* **2016**, *52*, 6431.

(28) Yong, Y.; Cheng, X. J.; Bao, T.; Zu, M.; Yan, L.; Yin, W.; Ge, C. C.; Wang, D. L.; Gu, Z. J.; Zhao, Y. L. Tungsten Sulfide Quantum Dots as Multifunctional Nanotheranostics for *In vivo* Dual-Model Image-Guided Photothermal/Radiotherapy Synergistic Therapy. *ACS Nano* **2015**, *9*, 12451−12463.

(29) Iyer, A. K.; Khaled, G.; Fang, J.; Maeda, H. Exploiting the Enhanced Permeability and Retention Effect for Tumor Targeting. *Drug Discovery Today* **2006**, *11*, 812−818.
(30) Rasheed, T.; Nabeel, F.; Raza, A.; Bilal, M.; Iqbal, H. M. N. Biomimetic Nanostructures/Cues as Drug Delivery Systems: A Review. *Mater. Today Chem.* **2019**, *13*, 147−157.
(31) Nikulshina, V.; Hirsch, D.; Mazzotti, M.; Steinfeld, A. CO_2 Capture from Air and Co-production of H_2 via the $Ca(OH)_2$-$CaCO_3$ Cycle Using Concentrated Solar Power-Themodynamic Analysis. *Energy* **2006**, *31*, 1715−1725.
(32) Migliardini, F.; De Luca, V.; Carginale, V.; Rossi, M.; Corbo, P.; Supuran, C. T.; Capasso, C. Biomimetic CO_2 Capture Using A Highly Thermostable Bacterial α-Carbonic Anhydrase Immobilized on A polyurethane Foam. *J. Enzyme Inhib. Med. Chem.* **2014**, *29*, 146−150.
(33) Feng, S. M.; Liu, D. D.; Feng, W. Y.; Feng, G. Q. Allyl Fluorescein Ethers as Promising Fluorescent Probes for Carbon Monoxide Imaging in Living Cells. *Anal. Chem.* **2017**, *89*, 3754−3760.
(34) Cheng, L.; Liu, J. J.; Gu, X.; Gong, H.; Shi, X. Z.; Liu, T.; Wang, C.; Wang, X. Y.; Liu, G.; Xing, H. Y.; Bu, W. B.; Sun, B. Q.; Liu, Z. PEGylated WS_2 Nanoseets as A Multifunctional Theranostic Agent fr *In vivo* Dual-Modal CT/Photoacoustic Imaging Guided Photothermal Therapy. *Adv. Mater.* **2014**, *26*, 1886−1893.
(35) Yong, Y.; Zhou, L. J.; Gu, Z. J.; Yan, L.; Tian, G.; Zheng, X. P.; Liu, X. D.; Zhang, X.; Shi, J. X.; Cong, W. S.; Yin, W. Y.; Zhao, Y. L. WS_2 Nanosheet as A New Photosensitizer Carrier for Combined Photodynamic and Photothermal Therapy of Cancer Cells. *Nanoscale* **2014**, *6*, 10394−10403.
(36) Wan, W. L.; Lin, Y. J.; Chen, H. L.; Huang, C. C.; Shih, P. C.; Bow, Y. R.; Chia, W. T.; Sung, H. W. *In Situ* Nanoreactor for Photosynthesizing H_2 Gas to Mitigate Oxidative Stress in Tissue Infammation. *J. Am. Chem. Soc.* **2017**, *139*, 12923−12926.
(37) Pathak, R. K.; Marrache, S.; Choi, J. H.; Berding, T. B.; Dhar, S. The Prodrug Platin-*A*: Simultaneous Release of Cisplatin and Aspirin. *Angew. Chem., Int. Ed.* **2014**, *53*, 1963−1967.
(38) Farr, T. D.; Lai, C. H.; Grünstein, D.; Orts-Gil, G.; Wang, C. C.; Boehm-Sturm, P.; Seeberger, P. H.; Harms, C. Imaging Early Endothelial Inflammation Following Stroke by Core Shell Silica Superparamagnetic Glyconanoparticles that Target Selectin. *Nano Lett.* **2014**, *14*, 2130−2134.
(39) Olivo, M.; Bhuvaneswari, R.; Lucky, S. S.; Dendukuri, N.; Soo-Ping Thong, P. Targeted Therapy of Cancer Using Photodynamic Therapy in Combination with Multi-Faceted Anti-Tumor Modalities. *Pharmaceuticals* **2010**, *3*, 1507−1529.
(40) Skobe, M.; Hawighorst, T.; Jackson, D. G.; Prevo, R.; Janes, L.; Velasco, P.; Riccardi, L.; Alitalo, K.; Claffey, K.; Detmar, M. Induction of Tumor Lymphangiogenesis by VEGF-C Promotes Breast Cancer. *Nat. Med.* **2001**, *7*, 192−198.

https://dx.doi.org/10.1021/acscentsci.9b01342
ACS Cent. Sci. 2020, 6, 555−565